ELSEVIER

Journal of Power Sources 113 (2003) 245–254

JOURNAL OF POWER SOURCES

www.elsevier.com/locate/jpowsour

Gas-diffusion approach to the kinetics of oxygen recombination in lead-acid batteries

A. Kirchev*, D. Pavlov, B. Monahov

CLEPS, Bulgarian Academy of Sciences, Sofia 1113, Bulgaria

Abstract

Diffusion of oxygen through the thin liquid film (TLF) covering the surface of the negative active mass (NAM) crystals and impeded charge transfer through the electric double layer (EDL) were assumed to be the rate limiting stages of the closed oxygen cycle in VRLAB. Based on the theory of colloid systems, the thickness of the TLF was determined and its dependence on pore radius and surface tension at the gas/electrolyte interface was estimated. The initial and boundary conditions were defined and Fick's equation was solved for this case. The diffusion kinetics results obtained explain the dependence of the recombination current on the metal surface on which the electrochemical reaction takes place, the thickness of the TLF, the concentration of oxygen at both film surfaces, and the time of polarization. Using the film thickness equation derived by the colloid chemistry theory, a general equation was developed which determines the oxygen recombination rate dependence on the thin liquid film parameters, NAM structure and polarization time. The validity of this equation was experimentally proved for low and high electrolyte saturation levels of the plates, as well as for negative plates produced employing various technologies. This equation makes it possible to draw conclusions about the possible ways of improvement of the efficiency of the oxygen cycle and about the technologies for negative plate production for VRLAB applications.

Keywords: VRLA batteries; Gas diffusion; Oxygen recombination

1. Introduction

The closed oxygen cycle (COC) comprises the following elementary processes:

(a) Oxygen evolution on the surface of the positive plate.
(b) Transport of O_2 through the AGM separator to the negative plate. Oxygen transport proceeds through gas channels in AGM when the electrolyte saturation in it is <96%.
(c) The lead particles in the negative plate are covered by a layer of electrolyte. The gas (O_2) must dissolve in this layer and the oxygen molecules must diffuse to the lead surface at which the reduction proceeds through accepting electrons. The concentration of oxygen in the sulfuric acid solution is about 8×10^{-7} mol cm^{-3}. The diffusion coefficient of O_2 is about $1-2 \times 10^{-5}$ cm s^{-1} (depending on acid concentration). This figure shows that the liquid layer covering the metal surface may slow down markedly the rate of the COC.
(d) Oxygen may react at the electrode surface following two different mechanisms:
   ○ Chemical one

$$Pb + \tfrac{1}{2}O_2 \rightarrow PbO \quad (a)$$

$$PbO + H_2SO_4 \rightarrow PbSO_4 + H_2O \quad (b)$$

$$PbSO_4 + 2H^+ + 2e^- \rightarrow Pb + H_2SO_4 \quad (c)$$

   ○ Electrochemical one

$$zO_2 + 4H^+ + 4e^- \rightarrow 2H_2O \quad (d)$$

(e) H_2O transport from the negative towards the positive plate.

The slowest elementary process of the COC has been the object of several studies:

- It has been assumed that the slowest stage of the COC is the diffusion through a liquid layer wetting the surface of the negative plate [1–4]. The authors investigate the case of constant gas volume and cell temperature. The pressure in the cell will increase until the valve opens. If the charging current is sufficiently high the gas pressure in

* Corresponding author.
E-mail address: a_kirchev@abv.bg (A. Kirchev).

0378-7753/02/$ – see front matter
PII: S0378-7753(02)00520-7

the cell in this case will be kept constant by the valve. On long overcharge when the state of charge (SOC) is 100%, the composition of the outgoing gas will rapidly reach a H_2:O_2 ratio of 2:1 [4].

- It has been established that the recombination rate depends but very slightly on the potential of the negative plate. The process of O_2 reduction at rotating disk electrodes is a diffusion limited one, it can be represented by the Levich's equation [5–8];
- The influence of H_2SO_4 concentration on the kinetics of O_2 reduction on lead electrodes was determined in [9];
- The transport of O_2 to the surface of the negative plate and the O_2 reduction process were investigated by mathematical models and computer simulations proposed by Bernardi and Carpenter [10], Newman and Tiedeman [11], and Gu et al. [12]. An important assumption in these computer simulations is the consideration of impeded charge transfer through the electric double layer (EDL) during oxygen reduction on the negative plate. This assumption improves markedly the match between the calculated and the experimental data in all three investigations [10–12]. The authors use different variants of the general Volmer's equation for describing the kinetics of oxygen reduction.
- A mechanism of the processes taking place during oxygen evolution on PbO_2 was proposed in [13,14].

The properties of the thin liquid film (TLF) of electrolyte covering the Pb surface and their impact on oxygen diffusion were not considered in the above studies. The aim of the present investigation is to determine the influence of the properties of the thin liquid film on the kinetics of oxygen diffusion and its reduction on the Pb surface.

2. Oxygen reduction processes taking place on the lead surface

We took the following features into account when considering the oxygen diffusion and reduction processes at the Pb surface:

(a) The negative plate is characterized by high porosity and large surface area (0.8 $m^2\ g^{-1}$). Under VRLAB operating conditions, the electrolyte saturation of the negative plate is less than 90%. The gas (O_2) will penetrate into the volume of NAM through the open gas macro pores of the plate.
(b) The thickness of the thin liquid film (TLF) depends on the capillary pressure in the open gas–liquid pores. Under the action of the capillary pressure the film covering the surface of the lead crystals in the PAM becomes thinner.
(c) Water is formed as a result of oxygen reduction. Thus, there is a tendency for the thickness of the TLF to increase depending on the rate of O_2 reduction.
(d) The diffusion transport of oxygen follows Fick's equation and depends on the diffusion coefficient of oxygen in the H_2SO_4 solution, on the concentration of oxygen on both phase boundaries of the TLF and on the thickness of the TLF.
(e) Oxygen diffusion through the TLF and charge transfer through the electric double layer (EDL) are the slowest steps of the process of reduction of oxygen molecules.
(f) NAM contains expanders (polymeric surfactants) which have an influence on the TLF and especially on the electric double layer at the metal surface. Thus expanders can influence the processes of oxygen reduction.

3. Evaluation of the TLF thickness and its influence on COC efficiency

The thickness of the thin liquid film h is a dynamic parameter which depends on both the changes in capillary pressure in the pores (tending to reduce h) and on the increased rate of recombination (generation of water, tending to increase h). The TLF thickness depends also on the nature of the expanders used which determine the surface tension, σ on the phase boundary gas–liquid. Under the influence of the above parameters the thickness of the TLF will tend to reach a certain steady state value. The latter will depend also on the electrolyte saturation level in the negative plate. The thickness can be estimated using the theoretical methods of colloid chemistry.

An open gas macropore in the negative plate is diagrammatically represented in Fig. 1. Such macropores are formed as a result of reduced electrolyte saturation in the negative plate. The capillary properties of the water solution open the pore and make its cross-section round shaped. Let us assume that a wetting film of electrolyte is formed between the pore wall and the lead crystal surface (Fig. 2).

A wetting film with thickness h is formed in a pore with radius R. The balance of forces on the curved meniscus area determines the capillary pressure P_σ in the pore, which is equal to $P_\sigma = P_1 - P_0$. P_1 is the pressure in the gas phase and P_0 the pressure in the liquid phase. The force balance on the gas/liquid interface of the film determines the disjoining pressure Π : $\Pi = P_1 - P_0$. At equilibrium $P_\sigma = \Pi$.

The stability conditions for such a wetting film can be calculated from the viewpoint of the so called DLVO theory (*Derjaguin*, *Landau*, *Verwey and Overbeek*) [15–19]. The stability of the film depends on the sign of the disjoining pressure Π, which is a basic thermodynamic characteristic of the TLF. Π accounts for the force of interaction between the two surfaces of the film.

The DLVO theory considers Π as a superposition of two basic universal molecular interactions, the electrostatic and the van der Waals ones:

$$\Pi = \Pi_{el} + \Pi_{VdW} \quad (1)$$

Because of the high H_2SO_4 concentration (about 5 mol/l) in the cell (and in the TLF) at 100% SOC, $\Pi_{el} = 0$. The van

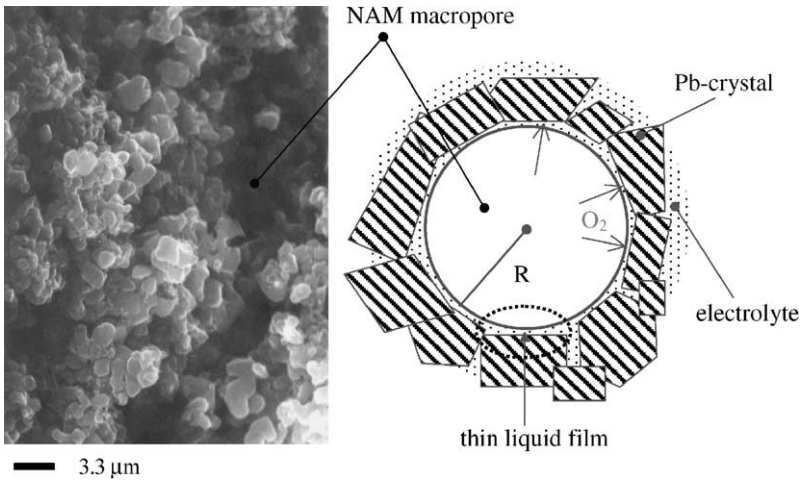

Fig. 1. Micrograph of an open gas pore in NAM and a scheme of the cross-section through the NAM pore.

der Waals's component Π_{VdW} can be calculated by the following equation:

$$\Pi_{\mathrm{VdW}} = -\frac{A_{\mathrm{H}}}{6\pi h^3} \tag{2}$$

where A_{H} is the Hamaker's constant of the three phase system (gas, electrolyte, lead). The Hamaker's constant A_{H} reflects the van der Waals's interaction between all molecules of the three phases in the system. In our case, A_{H} can be presented by the following equation:

$$A_{\mathrm{H}} = A_{\mathrm{el/el}} - A_{\mathrm{Pb/el}} \tag{3}$$

where the Hamaker's coefficient $A_{\mathrm{el/el}}$ accounts for the total interaction between the electrolyte molecules only, and $A_{\mathrm{Pb/el}}$ stands for the total interaction between the electrolyte molecules and the lead crystal atoms. It can be approximated that $A_{\mathrm{el/el}}$ is equal to the Hamaker's constant for water, which is about 4×10^{-13} erg. $A_{\mathrm{Pb/el}}$ (erg) can also be evaluated approximately using the equation

$$A_{\mathrm{Pb/el}} \approx (A_{\mathrm{el/el}} A_{\mathrm{Pb/Pb}})^{1/2} = 13 \times 10^{-13} \tag{4}$$

$A_{\mathrm{Pb/Pb}}$ is assumed to be about 40×10^{-13} erg. Hence, for A_{H} we obtain the value of $(-9) \times 10^{-13}$ erg. It must be pointed out that this value has a negative sign. According to

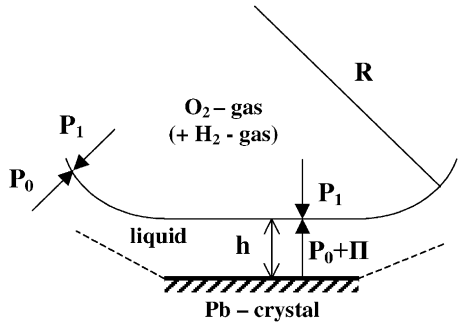

Fig. 2. Schematic representation of the balance of forces determining the stability of the wetting film formed in an open gas pore in NAM.

Eq. (2) we obtain the following term for the disjoining pressure:

$$\Pi_{\mathrm{VdW}} = \frac{3 \times 10^{-13}}{2\pi h^3} \tag{5}$$

The positive sign of Π means that there is a repulsive force between the two surfaces of the TLF, and hence the film can not rupture. Thus, the latter is thermodynamically stable. Once formed, the wetting film will get thinner with time under the action of the capillary pressure $P_\sigma = 2\sigma/R$, (R is the radius of the pore on whose wall the film is formed, and σ is the surface tension of the liquid phase).

Ignoring the influence of the water obtained on the film thickness, and assuming that the film is in a quasi-equilibrium state, $\Pi_{VdW} = P_\sigma = 2\sigma/R$. So for the thickness of the TLF we obtain:

$$h = \sqrt[3]{\frac{3 \times 10^{-13} R}{4\pi\sigma}} \tag{6}$$

This equation shows that h depends on the open pore radius R and on the surface tension σ. The latter depends on the presence of expanders. The thickness of the film decreases with decrease of R. When the film thickness becomes less than twice smaller than the diameter of one expander molecule, an additional repulsive force between the surfaces of the film will appear. This force is a result of the steric surface interactions between the expander molecules adsorbed at both interfaces. It stabilizes the thickness of the TLF [15–19].

For film thickness above 100 nm the interactive force between the two TLF surfaces weakens rapidly on increasing h and the film turns into a thick liquid layer. In the largest open pores, the diffusion transport of O_2 is very slow because of the great film thickness and small oxygen concentration gradient in it. Fig. 3 shows the dependence of the differential pore volume and of the pore surface as a function of pore radius for two negative plates used in this study. It is evident that the pores with the largest radii have the smallest

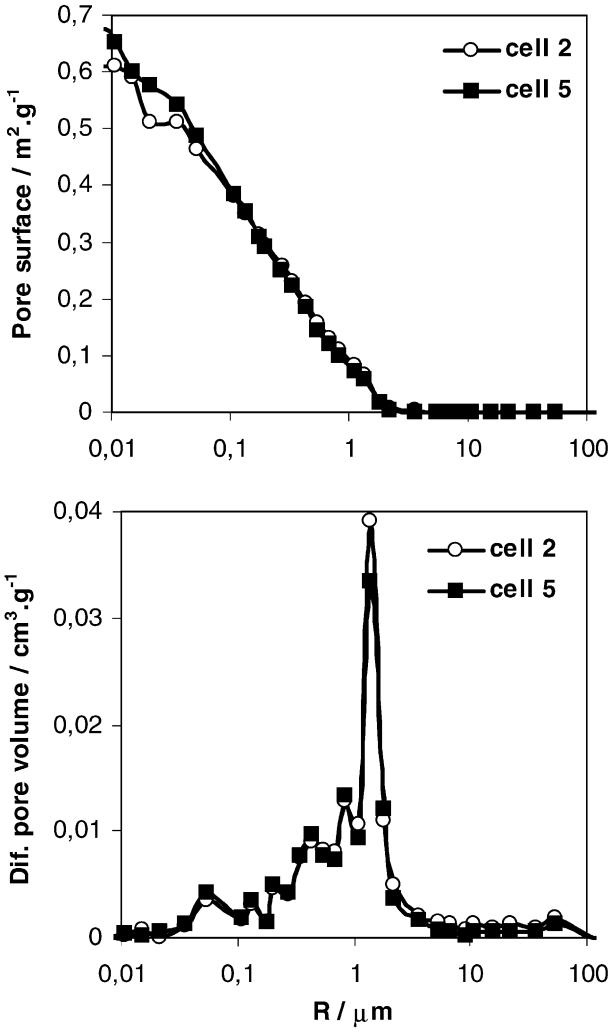

Fig. 3. Mercury porosimetric data for NAM sample from cell #2 (containing no additives) and from cell #5 (with a mixture of hydrophobic and hydrophilic additives).

share of the total gas–liquid surface area. This implies that recombination will proceed at the lowest rate in those pores due to the larger TLF thickness and to the smaller pore surface. Since at high electrolyte saturation of the negative plate only the largest pores are open, the COC efficiency in this case will be very low.

On decreasing the plate saturation, smaller and smaller pores are opened. Their surface is large, the capillary pressure in them is higher and the TLF thickness is small. Consequently, the O_2 concentration gradient, and hence the recombination rate, will increase. This is the reason why at lower electrolyte saturation in the plate the COC efficiency increases rapidly.

4. Processes taking place in the thin liquid film

Fig. 4 shows a scheme of the process of water production at the phase boundary metal/TLF according to the electro-

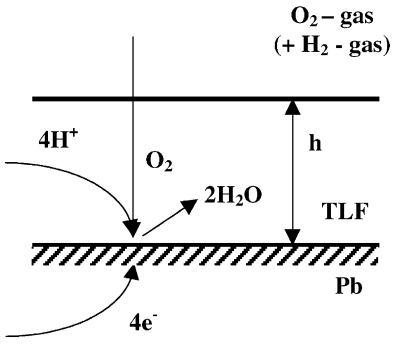

Fig. 4. Scheme of the electrochemical mechanism of O_2 reduction in the active centers at the phase boundary metal/TLF.

chemical mechanism of O_2 reduction. Oxygen diffusion through the wetting film on the NAM and impeded charge transfer through the EDL are assumed to be the rate-limiting steps of the oxygen cycle.

The diffusion of O_2 through the liquid film, the latter considered as two endless plane parallel surfaces with a distance h between them, is described by Fick's equation:

$$\frac{\partial c}{\partial t} = D\frac{\partial^2 c}{\partial x^2} \tag{7}$$

where D is the diffusion coefficient of O_2 in sulfuric acid solution (in $cm^2\ s^{-1}$) and c is the oxygen concentration (in mol cm^{-3}) in the TLF.

Let us formulate the initial and boundary conditions of oxygen diffusion. They are schematically represented in Fig. 5. We can assume as an initial condition the steady state distribution of oxygen concentration throughout the film, which is a consequence of galvanostatic polarization (I_1 = constant)

$$c(0,x) = \frac{c_1 - c_2}{h}x + c_2 \tag{8}$$

c_1 is the oxygen concentration at the phase boundary gas/TLF, and c_2 is the oxygen concentration at the phase boundary lead crystal/TLF. c_2 is not equal to 0 due to the

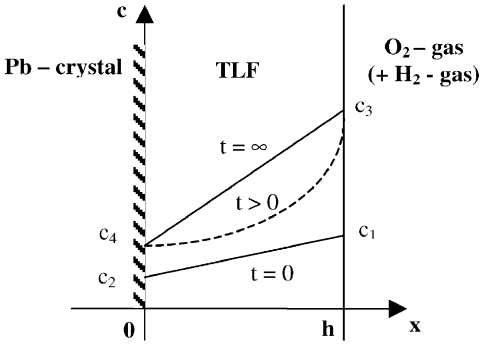

Fig. 5. Initial and boundary conditions for Fick's equation. The symbol c denotes the O_2 concentration (in mol cm^{-3}) in the electrolyte film, x and t are the direction and time, respectively. The dashed line illustrates a solution of Fick's equation at a moment of time $t > 0$.

fact that the kinetics of the oxygen reduction process is controlled by diffusion and impeded charge transfer.

If the current value increases from I_1 at $t = 0$ to I_2 at a moment $t > 0$ the boundary conditions are:

$$c(t,0) = c_4 \text{ and } c(t,h) = c_3 \tag{9}$$

where c_3 is the concentration of oxygen at the phase boundary gas/TLF, and c_4 is the concentration of oxygen at the phase boundary lead crystal/TLF at I_2. According to the general Volmer's equation on increasing the current that flows through the cell the concentration c_4 should also increase compared to c_2. However, due to the reduction of oxygen water is produced. If the water flow from the metal surface is sufficiently intense, the concentration change will be in the opposite direction, i.e. c_4 will decrease compared to c_2. These boundary conditions describe a new steady state distribution $c(x)$, which will be approached after a long enough time.

In order to solve the diffusion task, we use the integral transformation of Laplace at time t. The solution is the Laplace image of the dependence of the concentration on x and s, where s is the analog of time in the Laplace's space:

$$\hat{c}(s,x) = \left[\frac{(c_4 - c_2)ch[(x-h)\sqrt{s/D}] + (c_3 + c_1)ch(x\sqrt{s/D})}{sh(h\sqrt{s/D})} - \left(\frac{c_1 - c_2}{h}x + c_2\right)\right]\frac{1}{s} \tag{10}$$

The O_2 recombination current I_{rec} is equal to the O_2 flow which reached the phase boundary lead crystal/TLF, i.e. to the concentration gradient at this interface, which can be calculated from the derivative $(\partial\hat{c}/\partial x)$ at $x = 0$. Using the inverse Laplace transformation the following equation is obtained:

$$\frac{I_{rec}}{4F} = -SD\left(\frac{\partial c}{\partial x}\right)_{x=0} = SD\left(\frac{c_1 - c_2}{h} - \frac{c_4 - c_2}{\sqrt{\pi Dt}}\right) \tag{11}$$

where S is the surface area through which diffusion proceeds, F the Faraday's constant. The equation is obtained with the accuracy of an additive constant, since at $t \to \infty$ the gradient $(c_3 - c_4)$ should be considered instead of $(c_1 - c_2)$. $(c_3 - c_4)$ applies for the steady state kinetics at the higher current. That is why Eq. (11) should be represented as:

$$\frac{I_{rec}}{4F} = -SD\left(\frac{\partial c}{\partial x}\right)_{x=0} = SD\frac{c_3 - c_4}{h} - SD\frac{c_4 - c_2}{\sqrt{\pi Dt}} \tag{12}$$

As is evident, the recombination current is proportional to the thin liquid film surface through which oxygen diffuses. The larger this surface, the higher the recombination current and the COC efficiency. The second term in this equation is proportional to $t^{-1/2}$. During the initial moments of the process, when t is a very small number, $I_{rec} < 0$. For this case Eq. (12) does not have real meaning and I_{rec} should be considered equal to 0. After a certain time τ the second term of Eq. (12) becomes smaller than the first one and I_{rec} acquires a positive value.

Eq. (12) shows that the recombination rate I_{rec} depends largely on the TLF thickness h. The bigger the h value the smaller the oxygen reduction rate. Figs. 1 and 2 show that the TLF differs in thickness in the different areas of the pore. In the areas where the TLF is very thin (i.e. h is very small) the recombination rate will be very high, and in other areas where a thick TLF is formed, I_{rec} will be very small or tending to 0. This approach illustrates the fact, that oxygen reduction proceeds actually in a certain number of active centers where the TLF has a minimum thickness. Thus, the surface S should be considered as an effective sum of the areas of the active centers where oxygen reduction takes place.

Let us replace h from Eq. (12) with its equivalent determined for the TLF from Eq. (6). The following equation is obtained for I_{rec}:

$$v_{rec} = \frac{I_{rec}}{4F} = 2.37 \times 10^4 SD(c_3 - c_4)\sqrt[3]{\frac{\pi\sigma}{R}} - S(c_4 - c_2)\sqrt{\frac{D}{\pi t}} \tag{13}$$

where v_{rec} means the rate of O_2 flow, which recombines to H_2O. This is the general equation for the oxygen reduction rate, which accounts not only for the oxygen diffusion rate but also for the properties of the thin liquid film.

For a long enough time $t \to \infty$, the second additive term of Eq. (13) becomes very small and can be ignored. In this case the following equation is obtained for the steady state oxygen reduction rate:

$$\frac{I_{rec}}{4F} = 2.37 \times 10^4 SD(c_3 - c_4)\sqrt[3]{\frac{\pi\sigma}{R}} \tag{14}$$

The value of the steady state current is determined by the Pb crystal surface area on which the reduction proceeds, the pore radius and the surface tension at the boundary gas/TLF. These parameters depend on the negative active mass (NAM) structure and properties, and the kind of expander used for its preparation. There is also a second group of parameters characterizing the diffusion process in the thin liquid film. These are the oxygen concentrations on both phase boundaries and the diffusion coefficient of oxygen in the TLF.

5. Experimental

Fig. 6 presents a scheme of the material fluxes in a lead-acid cell with oxygen recombination for the case when the water decomposition current I is larger than that of oxygen recombination I_{rec} and part of the oxygen evolved on the positive plate leaves the cell at a rate I_{out}. Assuming that the cell is fully charged, the composition of the outgoing gas will consist of O_2 and H_2 in a volume ratio 1:2 considering Faraday's law.

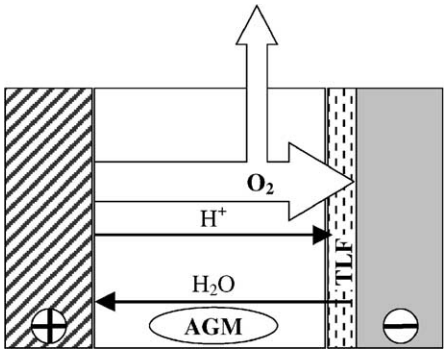

Fig. 6. Scheme of the material transport processes involved in the oxygen cycle.

Hence,

$$I = I_{rec} + I_{out} \tag{15}$$

when the cell is charged galvanostatically (I = constant)

The rate of the outgoing gas $v_{out} = I_{out}/4F$ (in mol s^{-1}) can be estimated by combining Eqs. (15) and (13):

$$v_{out} = \frac{I}{4F} - 2.37 \times 10^4 SD(c_3 - c_4)\sqrt[3]{\frac{\pi\sigma}{R}} + S(c_4 - c_2)\sqrt{\frac{D}{\pi t}} \tag{16}$$

As is evident from Eq. (16), v_{out} is a monotonously declining function of time. Two components of the rate v_{out} can be distinguished: first a non-steady state one, corresponding to the short period of time immediately after the current value changes from I_1 to I_2; and a second steady state one, corresponding to the case when $t \to \infty$.

5.1. Gassing rate monitoring system

In our laboratory a method was elaborated for determining the value of v_{out} through monitoring the number of gas bubbles leaving the cell per second [20]. A scheme of the gassing rate monitoring sensor is shown in Fig. 7. The outgoing gas is lead through the sensor forming gas bubbles in a tube filled with water. The gas bubbles are counted by a light source/photo detector couple. When a bubble is evolved it interrupts the light beam towards the photo detector. The pulse is detected and recorded by the PC. The system is calibrated by counting the number of bubbles

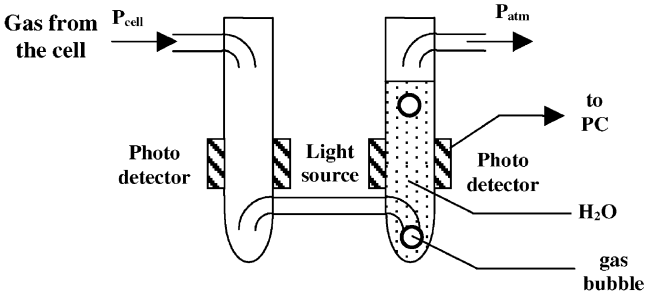

Fig. 7. Scheme of the gassing rate monitoring sensor.

corresponding to a gas volume of 100 cm^3 at an average rate of 2–3 bubbles per second. It has been estimated, that the average volume of one bubble is 0.2 cm^3. The relative error of the method is less than 10%. The rate of the outgoing gas v_{out} can be calculated according to the equation:

$$v_{out} = \frac{dn_{O_2}}{dt} = K\frac{dN}{dt} \tag{17}$$

where n_{O_2} is the number of oxygen moles leaving the cell and N the number of the bubbles detected by the monitoring system. K the constant of proportionality the value of which can be determined using the equation for the ideal gas $PV = nRT$. We assume that in our case the oxygen partial pressure accounts for one third of the outgoing gas pressure (which equals atmospheric), i.e. $P_{O_2} = P_{atm}/3$. In our experiment the volume of the outgoing gas is split into equal bubble volume portions, i.e. $V = NV_{bubble}$, where V_{bubble} is the average volume of a bubble as determined by the gassing rate monitoring system calibration. Hence, according to the ideal gas approach:

$$n_{O_2}RT = \frac{NP_{atm}V_{bubble}}{3} \tag{18}$$

Through differentiating this equation by time and regrouping the parameters we obtain

$$\frac{dN}{dt} = \frac{3RT}{V_{bubble}P_{atm}}\left(\frac{dn_{O_2}}{dt}\right) \tag{19}$$

Using Eq. (16) we come to:

$$\frac{dN}{dt} = \frac{3RT}{V_{bubble}P_{atm}}\left(\frac{I}{4F} - 2.37 \times 10^4 SD(c_3 - c_4)\sqrt[3]{\frac{\pi\sigma}{R}} + S(c_4 - c_2)\sqrt{\frac{D}{\pi t}}\right) \tag{20}$$

The method errors were minimized by integrating the gassing rate since the moment of applying the higher current I_2. Thus the dependence of the bubble number on t can be calculated from Eq. (20):

$$N(t) = \frac{3RT}{V_{bubble}P_{atm}}\left[\left(\frac{I}{4F} - 2.37 \times 10^4 SD(c_3 - c_4)\sqrt[3]{\frac{\pi\sigma}{R}}\right)t + \frac{3RT}{V_{bubble}P_{atm}}S(c_4 - c_2)\sqrt{\frac{Dt}{\pi}}\right] \tag{21}$$

Replacing:

$$a_1 = \frac{3RT}{V_{bubble}P_{atm}}S(c_4 - c_2)\sqrt{\frac{D}{\pi}} \tag{22a}$$

$$a_2 = \frac{3RT}{V_{bubble}P_{atm}}\left(\frac{I}{4F} - 2.37 \times 10^4 SD(c_3 - c_4)\sqrt[3]{\frac{\pi\sigma}{R}}\right) \tag{22b}$$

and

$$t = z^2 \tag{22c}$$

the cumulative number of bubbles up to the moment of time t is:

$$N(z) = a_2 z^2 + a_1 z \quad (23)$$

Presenting the experimental data as N versus $t^{1/2}$ (in $s^{1/2}$), a second order polynomial regression can be used for experimental evaluation of the constants a_1 and a_2.

5.2. Negative plates and cells

In order to estimate the influence of the surface tension at the gas/TLF boundary on the oxygen cycle efficiency we produced negative plates with two kinds of additives and with no additives. The plate dimensions were 53/65/2.5 mm. The plates were tank formed and dry charged. Experimental cells were assembled with one negative and two positive plates. The separator was AGM (Hollingsworth & Vose) 440 g m^{-2}. In order to obtain various AGM pore radii different compressions were applied to two of the cells. All cells were coupled to the gassing rate monitoring system. The potential of the negative plates versus a Hg/Hg_2SO_4 reference electrode was monitored in all cells. The cells were filled to the top with 1.27 specific gravity H_2SO_4 and left to soak for 30 min. After that the excess electrolyte was removed through 10 min draining. The cells were polarized on a BITRODE CN 25-12 testing module and, prior to the COC tests, the cells were conditioned by charging at 0.25 A for 2 h followed by 10 charge/discharge cycles (discharge: $I_d = 0.25$ A to $U_{cut\text{-}off} = 1.8$ VPC; charge: $I_{ch} = 0.25$ A, $U_{lim} = 2.53$ VPC), charge factor $\eta = 118\%$, and another 10 charge/discharge cycles with the same profile of charge/discharge.

6. Results and discussion

6.1. Polarization profiles

As established earlier using the same technique [20] when a current I_1 passes through a charged cell the cumulative gas bubble number leaving the cells features an abrupt initial increase (A) and then the rate of gassing decreases approaching an almost steady state value, as shown in Fig. 8. This initial rise was attributed to formation of gas channels through the AGM separator.

In this investigation our attention is focused on the phenomena that proceed in the negative plate after the gas channels are formed in the separator. For the purpose of this study, the cells were first polarized galvanostatically until a steady state gassing rate was obtained, i.e. all gas channels in the AGM separator were open. Then a new constant current value was applied (period (B) in Fig. 8), and the changes in gassing rate were recorded. We assume that the application of the new current does not cause any significant changes in the gas channels structure and the only phenomena that are affected by the current change are those that take place in the negative active mass (NAM),

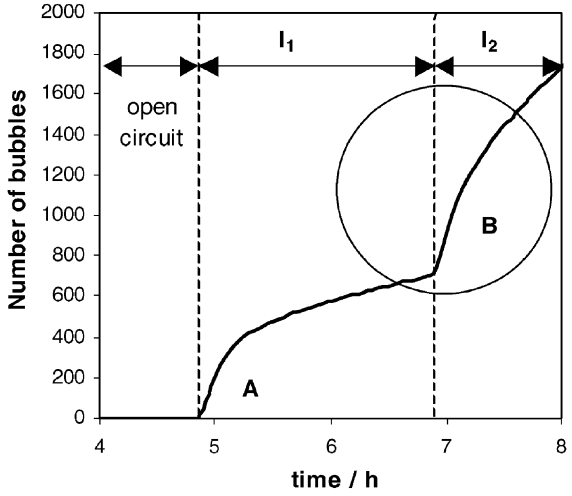

Fig. 8. Cumulative number of bubbles vs. time at polarization currents I_1 and I_2 ($I_1 < I_2$).

being related to oxygen reduction. These can be estimated indirectly from the changed rate of the gas flow leaving the cell. This change depends on the degree of saturation of NAM with electrolyte and on the new current value I_2.

In order to verify experimentally the validity of Eq. (20) we used two saturation levels and two I_2 current values.

H. High electrolyte saturation level of the plates and of the AGM separator, and a substantial current rise from $I_1 = 50$ mA to $I_2 = 150$ mA. In this case, the increased O_2 pressure in the separator at current I_2 forces the gas flow to penetrate into new pores of the negative plate. They have smaller radius R and when filled with oxygen they take part in the recombination process. Hence, the reaction surface S increases.

L. Low electrolyte saturation level of the active block and but a small current rise from $I_1 = 450$ mA to $I_2 = 500$ mA. In this case, no new gas pores are opened in NAM and R and S remain unchanged.

The investigation was performed using four kinds of negative plates with various surface tensions (σ) at the gas/electrolyte boundary. The following NAM additives were used:

(a) hydrophobic polymer—cell #6
(b) hydrophilic polymer—cell #4
(c) a mixture of hydrophobic and hydrophilic polymers—cell #5
(d) no NAM additives but different AGM compressions: 20% in cell #1 and 25% in cell #2

The cells were assembled into a battery and the latter was set to overcharge and COC studies were performed.

6.2. COC in cells with high H_2SO_4 saturation of the negative plate

Let us assume that V_{bubble} = constant irrespective of the gassing rate, D_{O_2} = constant since the cell is fully charged

and T = constant. In this case for Eq. (20) we obtain:

$$\frac{dN}{dt} = K_1 \frac{I}{P_{atm}} + K_2(c_4 - c_2)\frac{S}{P_{atm}}\sqrt{\frac{1}{t}} - K_3(c_3 - c_4)\frac{S}{P_{atm}}\sqrt[3]{\frac{\sigma}{R}} \quad (24)$$

where

$$K_1 = \frac{3RT}{4FV_{bubble}} \quad (25a)$$

$$K_2 = \frac{3RT}{V_{bubble}}\sqrt[3]{\frac{D}{\pi}} \quad (25b)$$

$$K_3 = 2.37 \times 10^4 \frac{3RTD}{V_{bubble}}\sqrt[3]{\pi} \quad (25c)$$

When the current value is changed from $I_1 = 50$ mA to $I_2 = 150$ mA the parameters R, S, $(c_3 - c_4)$ and, though less so, $(c_4 - c_2)$ will also change. σ is constant for this particular cell.

Fig. 9 presents the number of bubbles leaving the cell as a function of t for all five cells. What conclusions can be drawn based on the data in Fig. 9 and Eq. (24)? All curves rise initially and approach a steady state value. This indicates that after a certain non-steady state period of time the COC reaches a certain efficiency and gets into a steady state stage. What are the changes during the non-steady state period according to Eq. (21)? On raising the current the oxygen pressure at the boundary AGM/NAM increases. The gas penetrates into the pores with smaller radii (replacing the electrolyte) and thus the reaction surface S increases. According to Eq. (13), the increased S surface accelerates the rate of O_2 reduction. The O_2 concentration gradient $(c_3 - c_4)$ between the two TLF interfaces increases. Hence, the third term in Eq. (24) will acquire a value close to those of the other two terms. The difference between them determines the gassing rate dN/dt. The derivative decreases

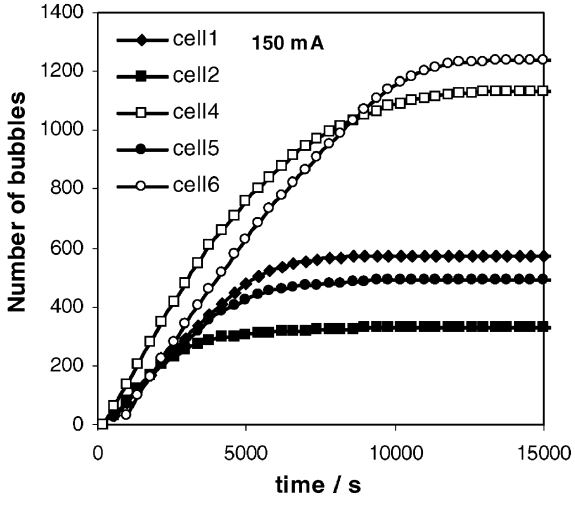

Fig. 9. Dependence of cumulative number of bubbles on time at $I = 150$ mA.

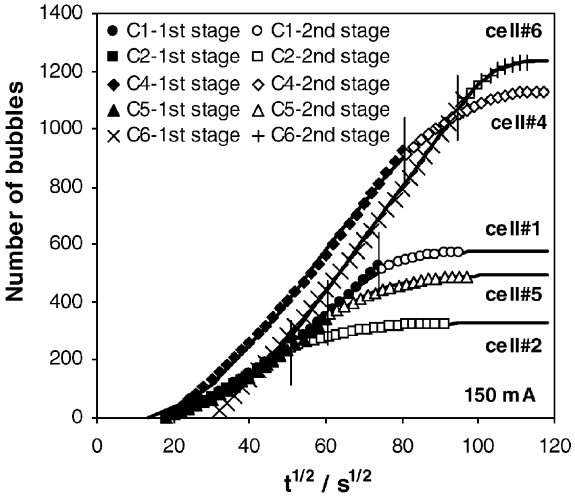

Fig. 10. Dependence of cumulative number of bubbles on the square root of time at $I = 150$ mA (solid lines) and results from the fit by Eq. (21) (symbols).

approaching 0. This is exactly the form of the experimental curves in Fig. 9.

What is the duration of the non-steady state stage and when will the steady state stage begin? This can be estimated by fitting the experimental data to Eq. (23).

The number of bubbles leaving each cell is shown in Fig. 10 as a function of the square root of time (s). The experimental data were fitted by a second order polynomial regression, which corresponds to Eq. (23), where N is the number of bubbles leaving the cell for the period of time between 0 and t. The coefficients a_1 and a_2 are related to the parameters presented in Eq. (22). The experimental data are illustrated by a solid line in the figure, and the best fit values calculated according to Eq. (21), by symbols. The symbols used for the first and the second stages are different, and the transition point is marked by a vertical line. The equation fits well all parts of the experimental data plot, the coefficients a_1 and a_2 have different values for the two stages. Their values for the non-steady state (I) and for the steady state (II) stages are given in Table 1.

According to Eq. (22a) the increase of a_1 in the second stage is due to the increase of the reaction area S where oxygen reduction proceeds. The data in Fig. 3 show that this area increases rapidly in the pores with smaller radii. The oxygen concentration difference $(c_4 - c_2)$ at the boundary metal/TLF also increases.

According to Eq. (22b), the fact that a_2 has a negative sign during the second stage indicates that S and $(c_3 - c_4)$ increase and R decreases. Hence $2.37 \times 10^{-4} SD(c_3 - c_4)\text{-}(\pi\sigma/R)^{1/3} > (I/4F)$ and $a_2 < 0$.

Fig. 9 shows that cell #6 with hydrophobic and cell #4 with hydrophilic polymer additives have the lowest COC efficiency. For cell #6, the transport of H^+ ions in the pores of NAM is impeded by the hydrophobic layer. In the negative plate of cell #4 the gas pores are blocked by the hydrophilic polymer and O_2 reaches only the largest pores

Table 1
a_1 and a_2 values for the polynomial regression in the case of high H_2SO_4 saturation level of the negative plate

Current	Stage	Coefficient	Cell 1	Cell 2	Cell 4	Cell 5	Cell 6
0.15 A (0.09 C)	1st stage	a_1 [$s^{-1/2}$]	2.97	2.37	8.05	0.98	10.19
		a_2 [s^{-1}]	0.070	0.073	0.071	0.092	0.052
	2nd stage	a_1 [$s^{-1/2}$]	28.06	9.56	41.48	20.54	116.96
		a_2 [s^{-1}]	−0.149	−0.053	−0.179	−0.107	−0.520

which have but a small surface. When both polymer additives are used in combination the obtained balance between the hydrophobic and hydrophilic properties of the surface causes a dramatic improvement in COC efficiency, which is observed in cell #5.

The cells with no additives (cell #1 and cell #2) have high COC efficiency. The latter is higher for the cell with higher compression, since the O_2 pressure inside the NAM pores is larger. The gas penetrates into the pores with smaller radii and the reaction surface S increases. Consequently, the COC efficiency improves. An interesting fact from a practical point of view is that the cell with a mixture of hydrophobic and hydrophilic polymer additives, and 20% compression (cell #5) has a higher COC efficiency than the cell under the same compression but with no additives (cell #1). This indicates that a proper selection of NAM additives with hydrophobic and hydrophilic properties can influence both σ and h (film thickness), and hence the COC efficiency.

6.3. COC in cells with low H_2SO_4 saturation level of the negative plate

The current value was changed from 450 to 500 mA. In this case, the pores with small radii are involved in the oxygen reduction process during the initial stage already (450 mA). The current rise does not affect the values of R and S. Since the current change is relatively small the pressure does not change either. σ remains constant, too. In this case Eq. (21) is reduced to:

$$\frac{dN}{dt} = K_1' I + K_2'(c_4 - c_2)\sqrt{\frac{1}{t}} - K_3'(c_3 - c_4)\sqrt[3]{\sigma} \qquad (26)$$

Fig. 11 presents the experimental data obtained as number of bubbles versus polarization time for $I = 500$ mA. When the saturation is low, the steady state stage is reached very quickly and the figure illustrates mainly this stage.

An analysis of the experimental curves considering Eq. (26) leads to the following conclusions. When the current rises from I_1 to I_2, the O_2 concentration difference at the two TLF surfaces increases due to the O_2 concentration rise at the boundary pore/TLF. This causes the oxygen reduction rate to increase. Water is formed and the TLF thickness grows causing a decrease of the rate of oxygen diffusion towards the metal surface and hence a decrease of the electrochemical reaction rate. Under the action of the capillary forces the TLF tends to get thinner. So after a certain period of time, a dynamic stage is reached when the differences $(c_3 - c_4)$ and $(c_4 - c_2)$ become constants. On the other hand, the second term in Eq. (26) becomes very small with time. It can be ignored because its value is much smaller than that of the first term. So $dN/dt = \text{constant}$. This is actually observed in Fig. 11, i.e. a linear increase of the cumulative number of bubbles with time.

Fig. 12 gives the dependence of the number of bubbles versus $t^{1/2}$. The experimental data are illustrated by a solid line, while the best fit values, calculated according to Eq. (21), are denoted by symbols. The experimental data fit well to Eq. (21) within the entire time range (12 h). The low electrolyte saturation of the NAM yields a system of gas pores with a large surface and a thin TLF. This ensures high COC efficiency for a long period of time.

Table 2 presents the values for a_1 and a_2 for the best fits calculated according to Eqs. (21) and (23).

Though the surface S is substantially larger in this case, the a_1 values are lower than those in Table 1 (Eq. (22a)). Probably, when the higher current I_2 is applied, the O_2 concentration on the lead surface does not change substantially and the concentration difference $(c_4 - c_2)$ is rather small. The value of a_1 remains very small.

The greater current value $I = 500$ mA makes the first term in Eq. (22b) greater than the second one and hence the sign of a_2 is positive.

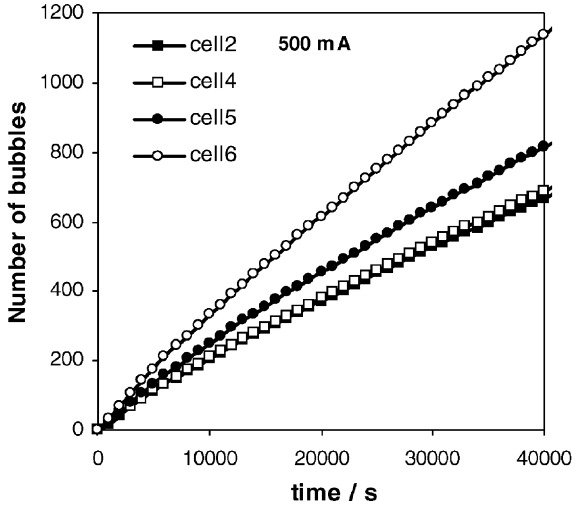

Fig. 11. Dependence of cumulative number of bubbles on time at $I = 500$ mA.

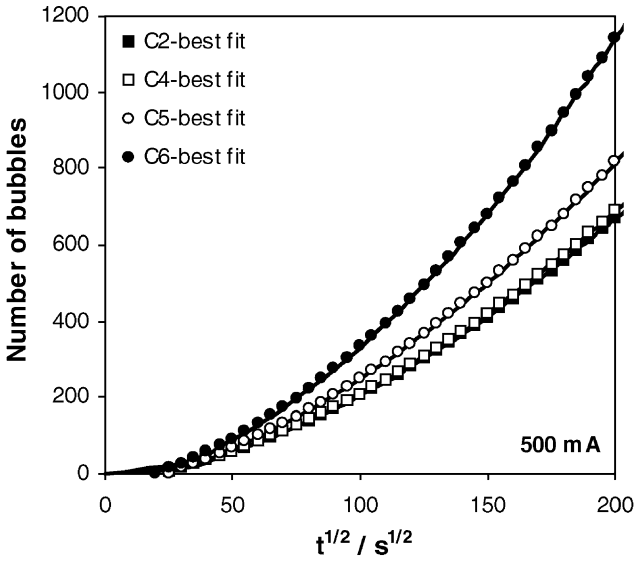

Fig. 12. Dependence of cumulative number of bubbles on the square root of time at $I = 500$ mA (solid lines) and results from the fit by Eq. (21) (symbols).

Table 2
a_1 and a_2 values for the polynomial regression in the case of a low H_2SO_4 saturation level of the negative plate

Current	Coefficient	Cell 2	Cell 4	Cell 5	Cell 6
0.50 A (0.31 C)	a_1 [$s^{-1/2}$]	1.29	1.17	1.63	1.51
	a_2 [s^{-1}]	0.0112	0.0121	0.0135	0.0220

The experimental data discussed above support the conclusions drawn from Eq. (21) thus providing an experimental proof of the model for oxygen diffusion and impeded charge transfer through a thin liquid film as the limiting stages of the processes involved in the closed oxygen cycle.

7. Conclusions

The aim of the present work was to study the processes taking place in the thin liquid film (TLF) that covers the Pb crystals of NAM. Oxygen diffusion through the TLF covering the NAM metal surface and impeded charge transfer through the electric double layer were assumed to be the rate-limiting steps of the oxygen cycle. These processes depend on the TLF properties, the structure of NAM and on the electrolyte saturation level of the plate.

Based on the colloid systems theory it has been established that the thickness of the TLF depends on pore radius and on the surface tension at the gas/liquid interface.

Solving Fick's equation for the defined initial and boundary conditions we obtained an equation giving the recombination current as a function of: the metal surface area on which recombination takes place, oxygen diffusion coefficient, thickness of TLF, oxygen concentration at the two TLF surfaces and polarization time.

Substituting the value for the TLF thickness by an expression based on colloid chemistry theory, a general equation was obtained for the relation between oxygen recombination rate and the properties of the TLF, NAM structure and time. The validity of this equation was proved experimentally for low and high electrolyte saturation levels of the plates and for negative plates containing hydrophilic and hydrophobic additives to NAM, as well as for two active block compressions. The experimental results are in perfect agreement with the conclusions drawn based on the model for the slowest stages of COC proposed in this work. This makes the model applicable to drawing practical conclusions about the methods to be used for improving the efficiency of the COC, and about the future trends in developing advanced negative plate technologies for VRLA batteries.

References

[1] M. Maja, N. Penazzi, J. Power Sources 25 (1989) 99.
[2] M. Maja, N. Penazzi, J. Power Sources 25 (1989) 229.
[3] S. Bodoardo, M. Maja, N. Penazzi, J. Power Sources 55 (1995) 183.
[4] F.E. Henn, C. Rouvet, A. de Guibert, Ph. Marteau, J. Power Sources 63 (1996) 235.
[5] E.A. Khomskaya, N.F. Gorbacheva, N.B. Tolochkov, Elektrokhimyia 16 (1980) 56.
[6] R.D. Armstrong, K.L. Bladen, J. Appl. Electrochem. 7 (1977) 345.
[7] N.A. Fleming, J.A. Harrison, J. Thompson, in: D.H. Collins (Ed.), Power Sources, Vol. 5, Academic Press, London, 1975, p. 23.
[8] C.S.C. Bose, A. Hampson, Bull. Electrochem. 4 (1988) 437.
[9] J. Mrha, K. Micka, J. Jindra, M. Musilova, J. Power Sources 27 (1989) 91.
[10] D.M. Bernardi, M.K. Carpenter, J. Electrochem. Soc. 142 (1995) 2631.
[11] J. Newman, W. Tiedemann, J. Electrochem. Soc. 144 (1997) 3081.
[12] W.B. Gu, G.Q. Wang, C.Y. Wang, J. Power Sources 108 (2002) 174.
[13] D. Pavlov, B. Monahov, J. Electrochem. Soc. 143 (1996) 3616.
[14] D. Pavlov, B. Monahov, J. Electrochem. Soc. 145 (1998) 70.
[15] D. Exerowa, P.M. Kruglyakov, Foam and Foam Films—Theory, Experiment and Application, Elsevier, Amsterdam, 1998, p. 150–166.
[16] B.V. Deriaguin, N.V. Churaev, Wetting Films, Nauka, Moscow, 1984.
[17] B.V. Deriaguin, Theory of Stability of Colloids and Thin Films, Consultants Bureau, New York, 1989.
[18] B.V. Deriaguin, N.V. Churaev, V.M. Muller, Surface Forces, Consultants Bureau, New York, 1987.
[19] J.N. Israelachvili, Intermolecular and Surface Forces, 2nd ed., Academic Press, London, 1985.
[20] D. Pavlov, S. Ruevski, V. Naidenov, G. Sheytanov, J. Power Sources 85 (2000) 164.